# Cluster properties from two-particle angular correlations in $p+p$ collisions at $\sqrt{s} = 200$ and 410 GeV

B. Alver,[4] B. B. Back,[1] M. D. Baker,[2] M. Ballintijn,[4] D. S. Barton,[2] R. R. Betts,[6] R. Bindel,[7] W. Busza,[4] Z. Chai,[2] V. Chetluru,[6] E. García,[6] T. Gburek,[3] K. Gulbrandsen,[4] J. Hamblen,[8] I. Harnarine,[6] C. Henderson,[4] D. J. Hofman,[6] R. S. Hollis,[6] R. Hołyński,[3] B. Holzman,[2] A. Iordanova,[6] J. L. Kane,[4] P. Kulinich,[4] C. M. Kuo,[5] W. Li,[4] W. T. LIn,[5] C. Lozides,[4] S. Manly,[8] A. C. Mignerey,[7] R. Nouicer,[2] A. Olszewski,[3] R. Pak,[2] C. Reed,[4] E. Richardson,[7] C. Roland,[4] G. Roland,[4] J. Sagerer,[6] I. Sedykh,[2] C. E. Smith,[6] M. A. Stankiewicz,[2] P. Steinberg,[2] G. S. F. Stephens,[4] A. Sukhanov,[2] A. Szopstak,[2] M. B. Tonjes,[7] A. Trzupek,[3] G. J. van Nieuwenhuizen,[4] S. S. Vaurynovich,[4] R. Verier,[4] G. I. Veres,[4] P. Walters,[8] E. Wenger,[4] D. Willhelm,[7] F. L. H. Wolfs,[8] B. Wosiek,[3] K. Woźniak,[3] S. Wyngaardt,[2] and B. Wysłouch[4]

[1]*Argonne National Laboratory, Argonne, Illinois 60439-4843, USA*
[2]*Brookhaven National Laboratory, Upton, New York 11973-5000, USA*
[3]*Institute of Nuclear Physics PAN, Kraków, Poland*
[4]*Massachusetts Institute of Technology, Cambridge, Massachusetts 02139-4307, USA*
[5]*National Central University, Chung-Li, Taiwan*
[6]*University of Illinois at Chicago, Chicago, Illinois 60607-7059, USA*
[7]*University of Maryland, College Park, Maryland 20742, USA*
[8]*University of Rochester, Rochester, New York 14627, USA*

(Received 6 April 2007; published 29 May 2007)

We present results on two-particle angular correlations in proton-proton collisions at center-of-mass energies of 200 and 410 GeV. The PHOBOS experiment at the BNL Relativistic Heavy Ion Collider has a uniquely large coverage for charged particles, giving the opportunity to explore the correlations at both short- and long-range scales. At both energies, a complex two-dimensional correlation structure in $\Delta\eta$ and $\Delta\phi$ is observed. In the context of an independent cluster model of short-range correlations, the cluster size and its decay width are extracted from the two-particle pseudorapidity correlation function and compared with previous measurements in proton-proton and proton-antiproton collisions, as well as PYTHIA and HIJING predictions.

DOI: 10.1103/PhysRevC.75.054913 PACS number(s): 25.75.Dw, 25.75.Gz

## I. INTRODUCTION

Studies of multiparticle correlations have proven to be a powerful tool in exploring the underlying mechanism of particle production in high energy hadronic collisions. Inclusive two-particle correlations have been found (e.g., Ref. [1]) to have two components: direct two-particle correlations as well as an effective "long-range" correlation due to event-by-event fluctuations of the overall particle multiplicity. By considering the two-particle rapidity density at fixed multiplicity, the intrinsic correlations between particles were isolated and found to be approximately Gaussian, with a range of $\sigma_\eta \sim 1$ unit in pseudorapidity [$\eta = -\ln(\tan(\theta/2))$]. Thus, these correlations have been conventionally called "short-range" correlations. Their properties have been explained by the concept of "cluster" emission.

The simple idea that hadrons are produced in clusters, rather than individually, has had great success in describing many features of particle production [1,2]. In a scenario of independent cluster emission, clusters are formed before the final-state hadrons and are independently emitted according to a dynamically generated distribution in $\eta$ and $\phi$. The clusters subsequently decay isotropically in their own rest frame into the observed final-state hadrons. An independent cluster emission model has been widely applied to the study of two-particle correlations [3,4], where the observed correlation strength and extent in phase space can be parametrized in terms of the cluster multiplicity or "size" (the average number of particles in a cluster) and the decay "width" (the separation of the particles in pseudorapidity). However, it should be noted that independent cluster emission is only a phenomenological approach which provides no insight into cluster production mechanisms. Further modeling will be required to connect these studies to the underlying QCD dynamics.

A related measurement, studying the forward-backward multiplicity correlations, was performed in Au+Au collisions at center-of-mass energy per nucleon pair ($\sqrt{s_{NN}}$) of 200 GeV using the PHOBOS detector at BNL's Relativistic Heavy Ion Collider (RHIC) [5]. The event-by-event observable $C = (N_F - N_B)/\sqrt{N_F + N_B}$ is constructed, where $N_F$ and $N_B$ are defined to be the total multiplicity in two symmetric regions forward and backward of midrapidity. The variance $\sigma_C^2$, which is related to the cluster size, was measured. An effective cluster size of approximately 2–3, increasing with the size of the pseudorapidity window, was observed. In heavy ion collisions at RHIC, it has been predicted that the formation of a quark gluon plasma (QGP) could modify cluster properties relative to $p+p$ collisions [6]. Unfortunately, the method used in Ref. [5] was found to have intrinsic limitations for measuring the properties of clusters emitted near midrapidity. This makes direct tests of these predictions difficult and suggests a need for different methods to access cluster properties directly.

To explore the properties of short-range correlations in more detail and to study cluster properties quantitatively, this paper presents the two-particle angular correlations in

 

$p$+$p$ collisions at c.m. energies ($\sqrt{s}$) of 200 and 410 GeV over a very broad acceptance in $\Delta\eta$ ($= \eta_1 - \eta_2$) and $\Delta\phi$ ($= \phi_1 - \phi_2$). The PHOBOS Octagon detector, covering pseudorapidity $-3 < \eta < 3$ over almost the full azimuth, is well suited to measuring the correlations between particles emitted from clusters, which have been found to extend up to $\Delta\eta =$ 2–3 units of pseudorapidity. The observed two-dimensional correlation function shows a complex correlation structure in the hadronic final state. In this analysis, both the cluster size and its decay width are extracted from the two-particle correlations as a function of $\Delta\eta$. Furthermore, the energy, multiplicity, and $\Delta\phi$ dependence of the cluster size and decay width are studied and compared with previous measurements as well as PYTHIA [7] and HIJING [8] predictions at various energies. Our present study in $p$+$p$ collisions will provide a useful baseline measurement for understanding the hadronization stage in $A$+$A$ collisions.

## II. DATA SETS

The data presented here for $p$+$p$ collisions at $\sqrt{s} = 200$ and 410 GeV were collected during RHIC runs 4 (2004) and 5 (2005) using the large-acceptance PHOBOS Octagon multiplicity detector covering pseudorapidity $-3 < \eta < 3$ over almost full azimuth. A full description of the PHOBOS detector can be found in Ref. [9]. Single diffractive $p$+$p$ events were suppressed by requiring at least one hit in each of two sets of 16 scintillator trigger counters located at distances of $-3.21$ m and 3.21 m from the nominal interaction point $z_{\rm vtx} = 0$ along the beam axis. They cover an acceptance of $3 < |\eta| < 4.5$ and $-180^\circ < \phi < 180^\circ$. About $5 \times 10^5$ 200-GeV and $8 \times 10^5$ 410-GeV $p$+$p$ events were selected for further analysis by requiring that the main collision vertex fell within $|z_{\rm vtx}| < 10$ cm along the beam axis.

The angular coordinates $(\eta, \phi)$ of charged particles are measured using the energy deposited in the silicon pads of the Octagon. The granularity of the Octagon is determined by the sizes of the readout pads, which are about $11.25^\circ$ ($\sim$0.2 radians) in $\phi$ and range from 0.006 to 0.05 in $\eta$. Monte Carlo (MC) studies using the PYTHIA event generator show that in the low-multiplicity $p$+$p$ environment, 98% of hits on adjacent pads in $\eta$ are created by single primary particles with a small angle of incidence. All such neighboring hits are merged to single hits in order to avoid fake particle pairs. Noise and background hits are rejected by cutting on the deposited energy corrected for the path length through the silicon after hit merging, assuming that the charged particle originated from the main vertex. Depending on $\eta$, the merged hits with less than 50–60% of the energy loss expected for a minimum ionizing particle are rejected. More details of the hit reconstruction procedure can be found in Ref. [10].

## III. DEFINITION OF TWO-PARTICLE CORRELATION FUNCTION

Following an approach similar to that in Ref. [2], the inclusive charged two-particle correlation function in two-particle $(\eta_1, \eta_2, \phi_1, \phi_2)$ space is defined as

$$R(\eta_1, \eta_2, \phi_1, \phi_2) = \left\langle (n-1)\left(\frac{\rho_n^{\rm II}(\eta_1, \eta_2, \phi_1, \phi_2)}{\rho_n^{\rm I}(\eta_1, \phi_1)\rho_n^{\rm I}(\eta_2, \phi_2)} - 1\right)\right\rangle, \tag{1}$$

where

$$\rho_n^{\rm I}(\eta, \phi) = \frac{1}{n\sigma_n}\frac{d^2\sigma_n}{d\eta\, d\phi}$$

is the single charged particle density distribution, and

$$\rho_n^{\rm II}(\eta_1, \eta_2, \phi_1, \phi_2) = \frac{1}{n(n-1)\sigma_n}\frac{d^4\sigma_n}{d\eta_1\, d\eta_2\, d\phi_1\, d\phi_2}$$

denotes the charged particle pair distribution. Here $\sigma_n$ is the cross section of observing $n$ charged particles. The above distributions obey the normalization relations

$$\int \rho_n^{\rm I}(\eta, \phi)\, d\eta\, d\phi = 1$$

and

$$\int \rho_n^{\rm II}(\eta_1, \eta_2, \phi_1, \phi_2)\, d\eta_1\, d\eta_2\, d\phi_1\, d\phi_2 = 1.$$

In practice, we concentrate on the difference in azimuthal angle and pseudorapidity between two particles. The correlation function in Eq. (1) is simplified by averaging over the full acceptance $-3 < \eta_1, \eta_2 < 3$ and $-180^\circ < \phi_1, \phi_2 < 180^\circ$, reducing the dimensionality of the parameter space to $\Delta\eta$ and $\Delta\phi$ with a range of $|\Delta\eta| < 6$ and $|\Delta\phi| < 180^\circ$:

$$R(\Delta\eta, \Delta\phi) = \left\langle (n-1)\left(\frac{\rho_n^{\rm II}(\Delta\eta, \Delta\phi)}{\rho^{\rm mixed}(\Delta\eta, \Delta\phi)} - 1\right)\right\rangle. \tag{2}$$

The pair distribution $\rho_n^{\rm II}(\Delta\eta, \Delta\phi)$ (with unit integral) is determined by taking particle pairs from the same event, then averaging over all events. The mixed-event background, $\rho^{\rm mixed}(\Delta\eta, \Delta\phi)$ (with unit integral), is constructed by randomly selecting single particles from two different events with similar vertex position, representing a product of two single particle distributions. The vertex bin size of 0.5 cm used in event mixing is mainly determined by the vertex resolution of the detector in $p$+$p$ collisions. Since the background is found to be multiplicity independent, we use the inclusive $\rho^{\rm mixed}(\Delta\eta, \Delta\phi)$ in our calculations of Eq. (2). The track multiplicity $n$ is introduced to compensate for trivial dilution effects from uncorrelated particles [2]. This stems from the fact that the number of uncorrelated pairs grows quadratically with $n$, while the number of correlated pairs grows only linearly.

## IV. CORRECTIONS AND SYSTEMATICS

The PHOBOS Octagon detector has a single layer of silicon, so it does not provide momentum, charge, or mass information for the observed particles. Thus, secondary effects such as $\delta$ electrons, $\gamma$ conversions, and weak decays cannot be directly rejected. These will contribute to correlations unrelated to those between primary hadrons and modify the

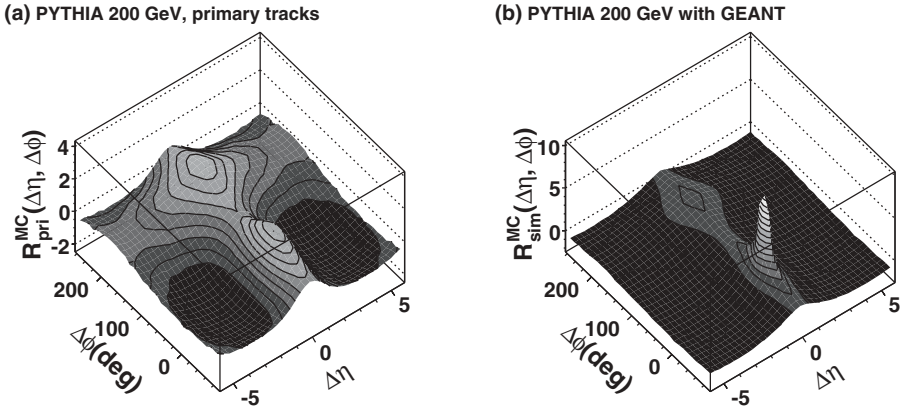


FIG. 1. Two-particle correlation function in $\Delta\eta$ and $\Delta\phi$ for (a) generator level PYTHIA for primary hadrons and (b) PYTHIA with full GEANT detector simulation and reconstruction procedures in $p+p$ collisions at $\sqrt{s} = 200$ GeV.

shape of the measured correlation function. The incomplete azimuthal acceptance in some pseudorapidity regions naturally suppresses the overall correlation strength, but MC simulations show that it does not change the shape of the correlation in $\Delta\eta$ and $\Delta\phi$. To correct for these detector effects in the data, correlation functions are calculated for PYTHIA events at $\sqrt{s} = 200$ GeV both at the generator level for true primary charged hadrons, $R^{\mathrm{MC}}_{\mathrm{pri}}(\Delta\eta, \Delta\phi)$ [Fig. 1(a)] and with the full GEANT detector simulation and reconstruction procedure, $R^{\mathrm{MC}}_{\mathrm{sim}}(\Delta\eta, \Delta\phi)$ [Fig. 1(b)]. As will be illustrated in Fig. 3, the actual information in $R(\Delta\eta, \Delta\phi)$ is reflected to the full $\Delta\eta$ and $\Delta\phi$ range in order to more clearly show the shape of the correlation function. The whole correction procedure can be summarized by the equation

$$R^{\mathrm{data}}_{\mathrm{final}}(\Delta\eta, \Delta\phi) = A \times \left[R^{\mathrm{data}}_{\mathrm{raw}}(\Delta\eta, \Delta\phi) - S(\Delta\eta, \Delta\phi)\right]. \quad (3)$$

The overall correlation structure consists of both intrinsic and secondary correlations, and these two sources of correlations are found to be largely independent of each other in MC studies, i.e., the correlation from secondaries is mostly determined by sensor thickness, detector geometry, known cross sections, and decay kinematics. First, within a narrow vertex range (2 cm), we compare the generator level MC correlation function excluding particles outside the PHOBOS detector acceptance, $R^{\mathrm{MC}}_{\mathrm{pri,acc}}(\Delta\eta, \Delta\phi)$, to the correlation function observed after processing the same MC events with all the primary hadrons through the GEANT simulation, $R^{\mathrm{MC}}_{\mathrm{sim}}(\Delta\eta, \Delta\phi)$ [Fig. 1(b)]. The difference between the two correlation functions, $S(\Delta\eta, \Delta\phi)$ [Fig. 2(b)], is attributed to the effects of secondary interactions, weak decays, and the reconstruction procedure, that is,

$$S(\Delta\eta, \Delta\phi) = R^{\mathrm{MC}}_{\mathrm{sim}}(\Delta\eta, \Delta\phi) - R^{\mathrm{MC}}_{\mathrm{pri,acc}}(\Delta\eta, \Delta\phi). \quad (4)$$

To estimate the suppression of the correlation strength due to limited acceptance, we compare $R^{\mathrm{MC}}_{\mathrm{pri}}(\Delta\eta, \Delta\phi)$ and $R^{\mathrm{MC}}_{\mathrm{pri,acc}}(\Delta\eta, \Delta\phi)$ using a $\chi^2$ test to extract a scaling factor $A$ for each vertex bin:

$$\chi^2 = \int \frac{\left[R^{\mathrm{MC}}_{\mathrm{pri}}(\Delta\eta, \Delta\phi) - A \times R^{\mathrm{MC}}_{\mathrm{pri,acc}}(\Delta\eta, \Delta\phi)\right]^2}{\sigma^{\mathrm{MC}}_{\mathrm{pri}}(\Delta\eta, \Delta\phi) \times A \times \sigma^{\mathrm{MC}}_{\mathrm{pri,acc}}(\Delta\eta, \Delta\phi)} d\Delta\eta\, d\Delta\phi, \quad (5)$$

where $\sigma^{\mathrm{MC}}_{\mathrm{pri}}(\Delta\eta, \Delta\phi)$ and $\sigma^{\mathrm{MC}}_{\mathrm{pri,acc}}(\Delta\eta, \Delta\phi)$ are the uncertainties of the correlation function $R^{\mathrm{MC}}_{\mathrm{pri}}(\Delta\eta, \Delta\phi)$ and $R^{\mathrm{MC}}_{\mathrm{pri,acc}}(\Delta\eta, \Delta\phi)$. Scaling factor $A$ is independent of $\Delta\eta$ and $\Delta\phi$ and is found to vary between 1.3 and 1.5 over the vertex range used in this analysis.

To get the final correlation function, $R^{\mathrm{data}}_{\mathrm{final}}(\Delta\eta, \Delta\phi)$, we apply Eq. (3) to the raw correlation function, $R^{\mathrm{data}}_{\mathrm{raw}}(\Delta\eta, \Delta\phi)$.

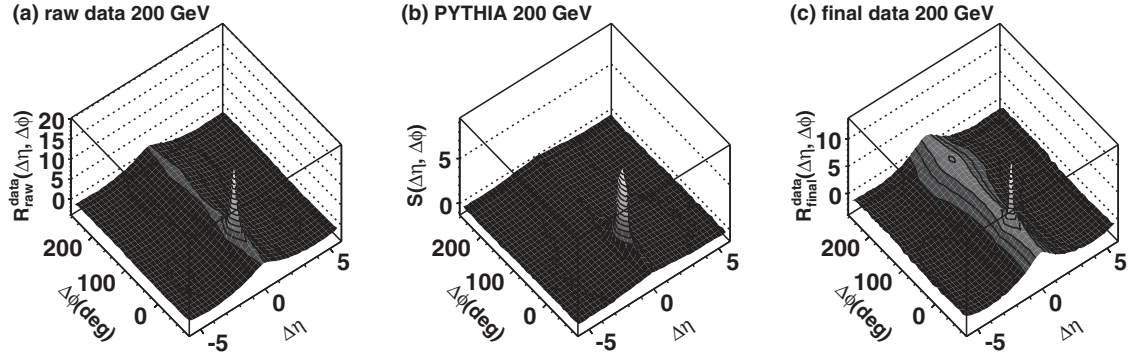


FIG. 2. Two-particle correlation function for $p+p$ collision data in $\Delta\eta$ and $\Delta\phi$ at $\sqrt{s} = 200$ GeV. (a) Raw data. (b) Correction function $S(\Delta\eta, \Delta\phi)$ from PYTHIA. (c) Final function.

The correction term $S(\Delta\eta, \Delta\phi)$ from Eq. (4) is used to subtract the effects of secondaries and weak decays, and scaling factor $A$ from the $\chi^2$ test in Eq. (5) is used to remove the suppression due to the holes in the PHOBOS acceptance. This procedure is done separately for each vertex bin. Three different MC generators are used to estimate the systematic uncertainties to the correlation function from this correction procedure, including PYTHIA, HIJING, and a modified PYTHIA in which all intrinsic correlations have been removed by performing event mixing at the primary hadron level (i.e., before weak decays). Typically the systematic error (biggest for the peak at $\Delta\eta = 0$ and $\Delta\phi = 0$) is less than 5%.

Both the correlation function for the data [Fig. 2(a)] and for the PYTHIA simulations [Fig. 1(b)] have a sharp peak at small $\Delta\eta$ and $\Delta\phi$, which is twice as high in the data as in the fully simulated MC events, but which is not present in the analysis using primary particles from the MC generator [Fig. 1(a)]. In the full GEANT simulations, the particles contributing to this peak are found to be mainly $\delta$ electrons (50%) and $\gamma$ conversions (40%). The width of the peak is about 0.3 in $\Delta\eta$ and $28^\circ$ in $\Delta\phi$ for both data and MC, indicating the same origin. However, the final data still contain a much narrower peak at the near side of $R^{\text{data}}_{\text{final}}(\Delta\eta, \Delta\phi)$ [Fig. 2(c)]. It is likely that this small angle structure results from background and detector effects which are not included in the MC simulation, although it is not possible to rule out unknown physics effects not implemented in the event generators. Since the physics of the clusterlike particle production investigated in this analysis is dominated by correlations on scales of approximately one unit in $\Delta\eta$, as will be shown later, we proceed by rejecting pairs in a small two-particle acceptance of $|\Delta\eta| < 0.15$ and $|\Delta\phi| < 5.625^\circ$ (the single bin centered at $\Delta\eta = 0$ and $\Delta\phi = 0$). Studies using primary particles from MC generators and the fully simulated events show that the extracted cluster parameters, described in the next section, change by less than 0.1% due to this cut.

In addition to the systematic errors related to the correction procedure, other systematic uncertainties are calculated by varying the vertex position and hit threshold cuts, and by studying the time dependence of the results within the two data sets. Since the acceptance of our detector is strongly dependent on vertex position, any systematic uncertainties due to acceptance and geometrical description should manifest themselves as a dependence of the final results on vertex position. The hit threshold cuts are used to discriminate between primary particles and noise or background hits; a variation of the thresholds allows us to test the impact of noise and background hits on the final results. For each selection of reconstruction parameters, a set of correlation functions are constructed under different conditions (i.e., ten different vertex positions) and fully corrected using the MC procedure described above. The rms of these correlation functions is calculated as an estimate of the systematic error from each particular source. The systematic errors due to the vertex position dependency, hit threshold cuts, and variations in different subsets of events are added in quadrature to get the total rms for each bin in $\Delta\eta$ and $\Delta\phi$. The vertex position dependency turns out to be the dominant source of the uncertainties. The final systematic uncertainties are quoted as 90% C.L.($1.6 \times$ rms).

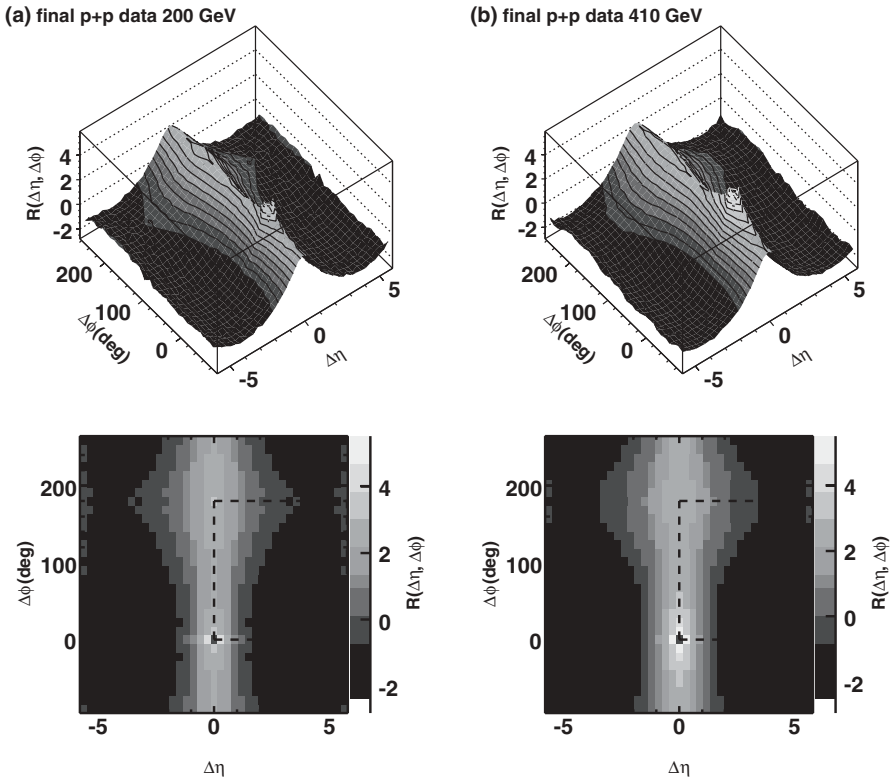


FIG. 3. Two-particle angular correlation function in $\Delta\eta$ and $\Delta\phi$ in $p$+$p$ collisions at $\sqrt{s} = 200$ GeV (column a) and 410 GeV (column b) (regions of $|\Delta\eta| < 0.15$ and $|\Delta\phi| < 5.625^\circ$ are excluded) shown in two types of representations. Areas enclosed by dashed lines on the lower panels indicate the actual information in the data which is then reflected to other regions to more clearly show the full shape of the correlation.

## V. RESULTS

The final two-particle inclusive correlation functions, averaged over ten vertex bins, are shown in Fig. 3 as a function of $\Delta\eta$ and $\Delta\phi$ at $\sqrt{s} = 200$ and 410 GeV. The near-side hole corresponds to the excluded region of $|\Delta\eta| < 0.15$ and $|\Delta\phi| < 5.625^\circ$. The systematic uncertainties in the absolute value of $R(\Delta\eta, \Delta\phi)$ are of the order of 0.3, relative to a peak value of 5, with little $\Delta\eta$ or $\Delta\phi$ dependence.

The complex two-dimensional correlation structure shown in Fig. 3 is approximately Gaussian in $\Delta\eta$ and persists over the full $\Delta\phi$ range, becoming broader toward larger $\Delta\phi$ (which will be discussed in quantitative detail below). Similar structures also exist in PYTHIA [Fig. 1(a)] though they do not reproduce the strength of the short-range rapidity correlations seen in the data. The qualitative features of the observed correlation structure are consistent with an independent cluster approach according to a simulation study from the CERN Intersecting Storage Rings (ISR) experiment using a low-mass resonance $(\rho, \omega, \eta)$ gas model [2]. The excess of the near-side peak ($\Delta\eta \sim 0$ and $\Delta\phi \sim 0$) relative to the away side could be partially a result of the Hanbury-Brown–Twiss (HBT) effect [11]. This possibility is investigated in the Appendix using a simple MC model and found to be negligible for the cluster properties investigated below.

To study the correlation structure quantitatively, the two-dimensional correlation function is projected into a one-dimensional pseudorapidity correlation function of $\Delta\eta$ by integrating $\rho_n^{\mathrm{II}}(\Delta\eta, \Delta\phi)$ and $\rho^{\mathrm{mixed}}(\Delta\eta, \Delta\phi)$ over $\Delta\phi$ as follows:

$$R(\Delta\eta) = \left\langle (n-1)\left(\frac{\int \rho_n^{\mathrm{II}}(\Delta\eta, \Delta\phi)\, d\Delta\phi}{\int \rho^{\mathrm{mixed}}(\Delta\eta, \Delta\phi)\, d\Delta\phi} - 1\right)\right\rangle. \quad (6)$$

The two-particle pseudorapidity correlation function $R(\Delta\eta)$, averaged over the $\Delta\phi$ range from $0^\circ$ to $180^\circ$, is shown in Fig. 4 at $\sqrt{s} = 200$ and 410 GeV. The error bars (also in Figs. 5–8) correspond to point-to-point systematic errors with 90% C.L. The error bands (also in Figs. 5–8) denote an overall scale error with 90% C.L. as an indication of the uncertainties in the correction method which tends to move all the data points up and down in a correlated fashion. The statistical errors are negligible because of the large $p$+$p$ event sample used in this analysis.

In the context of an independent cluster emission model, $R(\Delta\eta)$ takes the functional form [4]

$$R(\Delta\eta) = \alpha\left[\frac{\Gamma(\Delta\eta)}{\rho^{\mathrm{mixed}}(\Delta\eta)} - 1\right] \quad (7)$$

where the correlation strength $\alpha = \frac{\langle K(K-1)\rangle}{\langle K\rangle}$ is a parameter containing information on the distribution of cluster size $K$. The function $\Gamma(\Delta\eta)$ is a Gaussian function

$$\propto \exp[-(\Delta\eta)^2/(4\delta^2)]$$

characterizing the correlation of particles originating from a single cluster, where $\delta$ indicates the decay width of the clusters. The background distribution $\rho^{\mathrm{mixed}}(\Delta\eta)$ is just the distribution obtained by the event mixing introduced in Sec. III. To correct for the holes in the PHOBOS accep-

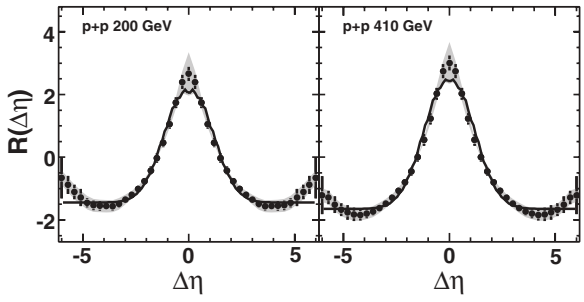


FIG. 4. Two-particle pseudorapidity correlation function, averaged over the $\Delta\phi$ range from $0^\circ$ to $180^\circ$, in $p$+$p$ collisions at $\sqrt{s} = 200$ and 410 GeV. Solid curves correspond to the fits by the cluster model using Eq. (7) over the full $\Delta\eta$ range. Error bars and bands correspond to point-to-point systematic errors and overall scale errors, respectively, with 90% C.L. Statistical errors are negligible.

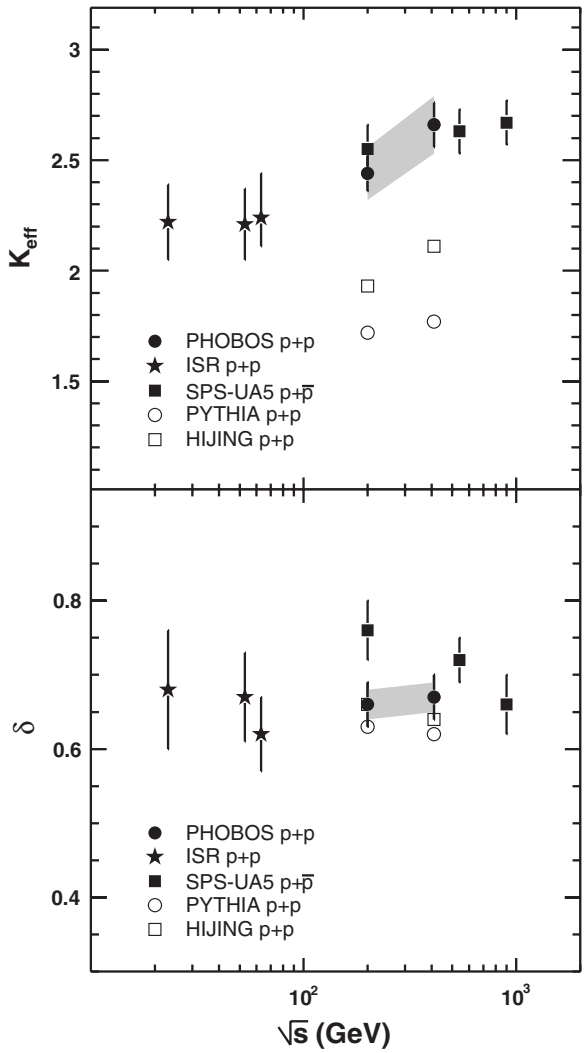


FIG. 5. $K_{\mathrm{eff}}$ and $\delta$ as functions of $\sqrt{s}$ measured by PHOBOS, UA5 [1], and ISR [2,12] experiments for $p$+$p$ and $p + \bar{p}$ collisions. PYTHIA and HIJING results are included. Error representations are the same as in Fig. 4.

tance, we calculate the ratio of the background for PYTHIA primary particles, $\rho^{\text{mixed}}_{\text{MC, pri}}(\Delta\eta)$, to the one obtained in the full GEANT simulations, $\rho^{\text{mixed}}_{\text{MC,sim}}(\Delta\eta)$. The ratio is applied to the background calculated from the data, $\rho^{\text{mixed}}_{\text{data,raw}}(\Delta\eta)$, as a multiplicative factor:

$$\rho^{\text{mixed}}_{\text{data,final}}(\Delta\eta) = \frac{\rho^{\text{mixed}}_{\text{MC, pri}}(\Delta\eta)}{\rho^{\text{mixed}}_{\text{MC,sim}}(\Delta\eta)} \times \rho^{\text{mixed}}_{\text{data,raw}}(\Delta\eta). \quad (8)$$

The effective cluster size is related to the extracted correlation strength via the relation

$$K_{\text{eff}} = \alpha + 1 = \frac{\langle K(K-1)\rangle}{\langle K\rangle} + 1 = \langle K\rangle + \frac{\sigma_K^2}{\langle K\rangle}. \quad (9)$$

Without any knowledge of the distribution of $K$, it is impossible to directly measure the average cluster size $\langle K\rangle$. However, by a $\chi^2$ fit of Eq. (7) to the measured two-particle pseudorapidity correlation function, the effective cluster size $K_{\text{eff}}$ and decay width $\delta$ can be estimated. The independent cluster model provides a good fit to the data over a large range in $\Delta\eta$, as shown in Fig. 4. An effective cluster size $K_{\text{eff}} = 2.44 \pm 0.08$ and width $\delta = 0.66 \pm 0.03$ for $\sqrt{s} = 200$ GeV and $K_{\text{eff}} = 2.66 \pm 0.10$, $\delta = 0.67 \pm 0.03$ for $\sqrt{s} = 410$ GeV are obtained with scale errors of 5% for $K_{\text{eff}}$ and 3% for $\delta$. The three most central points always lie above the fits, which could be due to residual secondary effects which are left uncorrected or other physics at this small scale in $\Delta\eta$. All fit results include these three points, but excluding them from the fit affects $K_{\text{eff}}$ and $\delta$ by no more than 3%.

In Fig. 5, our data are compared with previous measurements of $K_{\text{eff}}$ and $\delta$ as a function of $\sqrt{s}$. At lower ISR energies [2,12], $K_{\text{eff}}$ is constant within error bars. At the higher energies available at the CERN Super Proton Synchrotron (SPS) [1], the UA5 Collaboration finds $K_{\text{eff}}$ to be larger than at the ISR, but with little energy dependence between 200 and 900 GeV. The PHOBOS data are in good agreement with the UA5 measurements and, with much higher statistics in the $p$+$p$ event sample, show a clear energy dependence of $K_{\text{eff}}$. In contrast, the cluster decay width $\delta$ remains almost constant over the full range of collision energies. The event generators HIJING and PYTHIA show a similar energy dependence of $K_{\text{eff}}$

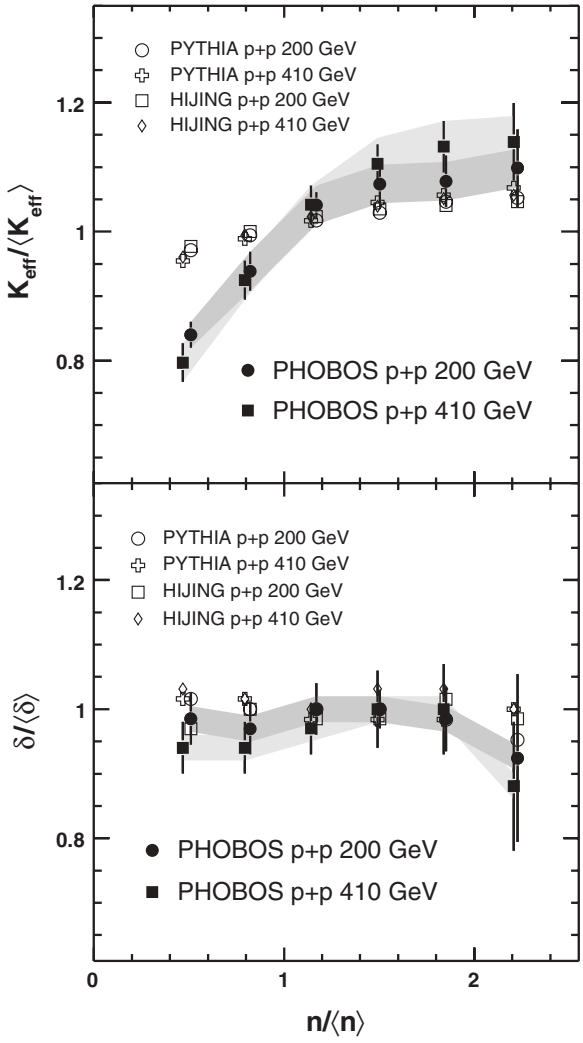


FIG. 6. Normalized effective cluster size $K_{\text{eff}}/\langle K_{\text{eff}}\rangle$ and decay width $\delta/\langle\delta\rangle$ as functions of normalized multiplicity $n/\langle n\rangle$ in $p$+$p$ collisions at $\sqrt{s} = 200$ and 410 GeV measured by PHOBOS and results of MC studies. Error representations are the same as in Fig. 4.

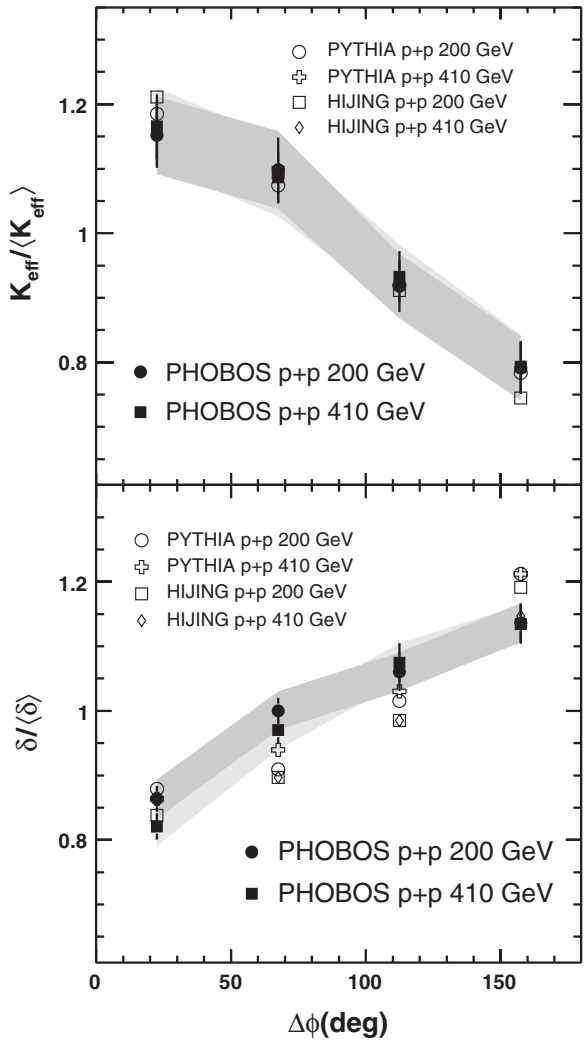


FIG. 7. Same as Fig. 6, but as function of $\Delta\phi$.

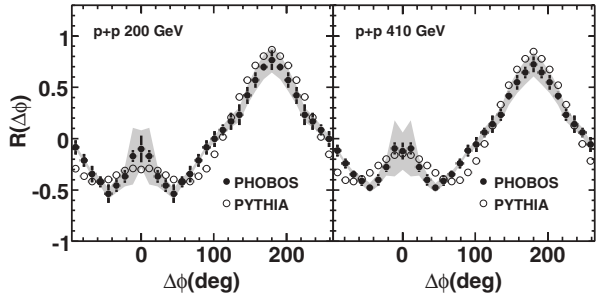


FIG. 8. Two-particle azimuthal correlation function, averaged over $\Delta\eta$ range 0–6, in $p$+$p$ collisions at $\sqrt{s} = 200$ and 410 GeV from PHOBOS and MC studies. Error representations are the same as in Fig. 4.

and $\delta$ to the data, but with a significantly lower magnitude of $K_{\text{eff}}$.

The observed cluster size cannot be fully explained by a resonance decay model even at very low energies, since the expectation of $\langle K \rangle$ from resonance decays is about 1.5 (extrapolating to 1.7 for $K_{\text{eff}}$ depending on the assumed cluster size distribution [1]). This is significantly lower than the observed values, but it is close to what is seen in PYTHIA. The HBT effect, after averaging over $\Delta\phi$, would increase the cluster size by no more than 2% (see Appendix). Additional sources of short-range correlations, such as local quantum number conservation [13], are needed to describe the data. As the energy increases, the onset of jets should play a more important role in the particle production giving bigger clusters, which could be the underlying cause for the observed energy dependence of $K_{\text{eff}}$. At the CERN Large Hadron Collider (LHC) , with $p$+$p$ collisions at $\sqrt{s} = 14$ TeV, jetlike particle production is expected to be dominant and should manifest itself in a further increase in the effective cluster size.

To gain further detailed information, the normalized cluster parameters $K_{\text{eff}}/\langle K_{\text{eff}} \rangle$ and $\delta/\langle\delta\rangle$ are calculated as a function of the normalized charged multiplicity $n/\langle n \rangle$ at $\sqrt{s} = 200$ and 410 GeV (Fig. 6). Scaled by the average charged multiplicity $\langle n \rangle$, the distribution of $n/\langle n \rangle$ turns out to be essentially identical for data and charged primary tracks from MC (PYTHIA and HIJING), despite the holes in the PHOBOS Octagon detector. By dividing the cluster parameters at different multiplicity by the averaged values, a scaling behavior is observed between two different energies in both data and MC.

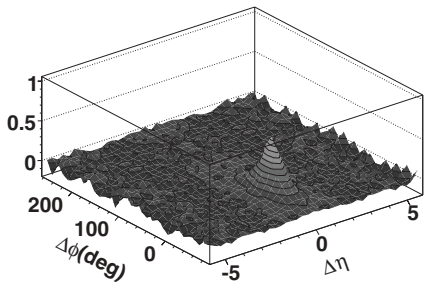


FIG. 9. Difference of correlation function with HBT weighting minus the one without HBT weighting in $\Delta\eta$ and $\Delta\phi$ for PYTHIA at $\sqrt{s} = 200$ GeV.

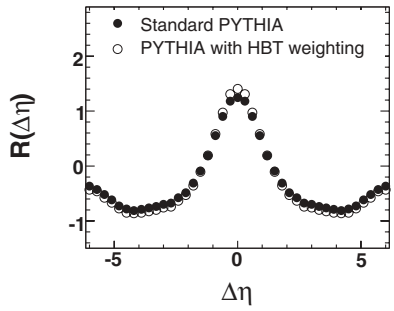


FIG. 10. Comparison of pseudorapidity correlation function with and without HBT weighting for PYTHIA at $\sqrt{s} = 200$ GeV.

$K_{\text{eff}}/\langle K_{\text{eff}} \rangle$ increases with event multiplicity, while $\delta/\langle\delta\rangle$ is found to be largely independent of it. PYTHIA and HIJING give a similar multiplicity dependence, but the increase in $K_{\text{eff}}/\langle K_{\text{eff}} \rangle$ is not as strong as in the data. Measurements from the ISR and UA5 experiments [1,2,12,14] are qualitatively consistent with PHOBOS but significantly limited by statistics, so they are not shown here.

To explicitly show the $\Delta\phi$ dependence of the short-range pseudorapidity correlation seen in Fig. 3, the $\Delta\phi$ range from $0^\circ$ to $180^\circ$ is divided into four regions and projected separately onto the $\Delta\eta$ axis. Figure 7 shows $K_{\text{eff}}/\langle K_{\text{eff}} \rangle$ and $\delta/\langle\delta\rangle$ for different $\Delta\phi$ regions. $K_{\text{eff}}/\langle K_{\text{eff}} \rangle$ gradually decreases while $\delta$ increases as one goes from small to large $\Delta\phi$ region. This might reflect some information about the transverse momentum distribution of the clusters [2]. High-$p_T$ clusters should generally contribute to a narrow hump in the near side (near $\Delta\phi = 0^\circ$) of the correlation function in Fig. 3, whereas the broader away side (near $\Delta\phi = 180^\circ$) comes from clusters with lower transverse momentum. Again, PYTHIA and HIJING results are qualitatively similar to the data but show a smaller decay width at intermediate $\Delta\phi$ and a larger decay width near $\Delta\phi = 180^\circ$.

The two-particle azimuthal correlation functions $R(\Delta\phi)$, averaged over a broad range of $\Delta\eta$ from 0 to 6, in $p$+$p$ collisions at $\sqrt{s} = 200$ and 410 GeV are presented in Fig. 8. $R(\Delta\phi)$ is obtained using a procedure similar to that shown for $R(\Delta\eta)$ in Eq. (6). The observed asymmetric structure in $\Delta\phi$ (with the $\Delta\eta$-averaged away-side peak larger than the near-side peak) could also provide some information about the momentum and size distribution of clusters. The $\Delta\eta$ integrated correlation function is similar in magnitude both for data and PYTHIA, despite the significant difference in the extracted $K_{\text{eff}}$. More detailed modeling of the cluster properties is needed to fully explain many aspects of the complex two-particle correlation function.

## VI. CONCLUSION

PHOBOS has measured two-particle angular correlations over a wide range in $\Delta\eta$ and $\Delta\phi$ in $p$+$p$ collisions at $\sqrt{s} = 200$ and 410 GeV. Short-range correlations are observed over the full range in $\Delta\phi$, with a maximum at $\Delta\eta = 0$ which becomes wider at larger $\Delta\phi$. In the context of the cluster model, the effective cluster size and decay width are extracted

from the two-particle pseudorapidity correlation function and compared with previous experiments as well as with the results of the HIJING and PYTHIA event generators. Dependence of the cluster size on both beam energy and scaled multiplicity is observed, while the cluster width is essentially constant. The short-range correlation strength (or equivalently the effective cluster size, $K_{\rm eff}$) exceeds the expectation from the decays of resonance particles, suggesting the need for other sources of short-range correlations. As mentioned in the Introduction, cluster properties could be modified in $A+A$ collisions relative to $p+p$ collisions by the presence of a QGP [6]. Future studies should clarify the evolution of cluster parameters from $p+p$ to $d$ + Au and $A+A$ collisions at RHIC energies.

## ACKNOWLEDGMENTS

We acknowledge the generous support of the Collider-Accelerator Department. This work was partially supported by U.S. DOE Grant Nos. DE-AC02-98CH10886, DE-FG02-93ER40802, DE-FC02-94ER40818, DE-FG02-94ER40865, DE-FG02-99ER41099, and W-31-109-ENG-38, by U.S. NSF Grant Nos. 9603486, 0072204, and 0245011, by Polish KBN Grant No. 1-P03B-062-27(2004-2007), by NSC of Taiwan Contract No. NSC 89-2112-M-008-024, and by Hungarian OTKA Grant No. F-049823.

## APPENDIX: HBT CORRELATIONS

The Bose-Einstein or HBT correlation will certainly contribute to the two-particle angular correlation function and thus might impact the estimation of cluster parameters [11]. It is known to cause a strong correlation between two identical particles having small relative invariant four-momentum $\mathbf{q}^2_{\rm inv}$ $[=(\mathbf{q}_1 - \mathbf{q}_2)^2]$. For identical bosons, the overall shape of the HBT effect can be approximated by a one-dimensional Gaussian correlation function

$$C(\mathbf{q}_{\rm inv}) = 1 + \lambda e^{-\mathbf{q}^2_{\rm inv} R^2_{\rm inv}}. \tag{10}$$

To estimate the effect of the HBT correlation in PYTHIA, which does not include this effect, we calculate the $\mathbf{q}_{\rm inv}$ for each pair in $\rho_n^{\rm II}(\Delta\eta, \Delta\phi)$ (ignoring the particle species), and weight the pair by $C(\mathbf{q}_{\rm inv})$ to artificially introduce the HBT correlation. In our study, we use $\lambda = 0.8$ and $R_{\rm inv} = 1.0$ fm. Considering that most of the pairs measured in this analysis are not identical-particle pairs, which should reduce the magnitude of $\lambda$, this choice of parameters exaggerates the expected effect of the HBT correlation. Thus, it gives a conservative estimate of its potential effect on the data.

In Fig. 9, the difference between the correlation function with and without $C(\mathbf{q}_{\rm inv})$ weighting is shown as a function of $\Delta\eta$ and $\Delta\phi$ for PYTHIA. Finally, Fig. 10 shows a comparison of pseudorapidity correlation functions with and without HBT weighting, with extracted cluster sizes of 1.76 and 1.72, respectively. From these studies, it appears that the HBT effect does enhance the short-range correlations with a range of around one unit in $\Delta\eta$ and 45° in $\Delta\phi$. However, after averaging over $\Delta\phi$, it only slightly influences the rapidity correlation function, resulting in an increase in cluster size of at most 2%. Even in the region $0° < \Delta\phi < 45°$, the increase is less than 3.5%.

[1] R. E. Ansorge *et al.* (UA5 Collaboration), Z. Phys. C **37**, 191 (1988).
[2] K. Eggert *et al.*, Nucl. Phys. **B86**, 201 (1975).
[3] F. Henyey, Phys. Lett. **B45**, 469 (1973); E. L. Berger, Nucl. Phys. **B85**, 61 (1975); J. L. Meunier and G. Plaut, *ibid.* **B87**, 74 (1975); C. Michael, *ibid.* **B103**, 296 (1976).
[4] A. Morel and G. Plaut, Nucl. Phys. **B78**, 541 (1974).
[5] B. B. Back *et al.*, Phys. Rev. C **74**, 011901(R) (2006).
[6] L. J. Shi and S. Jeon, Phys. Rev. C **72**, 034904 (2003).
[7] T. Sjostrand, S. Mrenna, and P. Skands, J. High Energy Phys. 05 (2006) 26. Version 6.325, single diffractive process excluded.
[8] M. Gyulassy and X. N. Wang, Comput. Phys. Commun. B **83**, 307 (1994). Version 1.383, single diffractive process excluded.
[9] B. B. Back *et al.*, Nucl. Instrum. Methods Phys. Res. A **499**, 603 (2003).
[10] Pradeep Sarin, Ph.D. thesis, Massachusetts Institute of Technology, 2003.
[11] C. Albajar *et al.*, Phys. Lett. **B226**, 410 (1989).
[12] D. Drijard *et al.*, Nucl. Phys. **B155**, 269 (1979).
[13] R. J. Porter and T. A. Trainor, Acta. Phys. Pol. B **36**, 353 (2005).
[14] W. Bell *et al.*, Z. Phys. C **22**, 109 (1984).